Capillary Leveling of Freestanding Liquid Nanofilms

Mark Ilton,[1] Miles M. P. Couchman,[1] Cedric Gerbelot,[2] Michael Benzaquen,[2] Paul D. Fowler,[1] Howard A. Stone,[3] Elie Raphaël,[2] Kari Dalnoki-Veress,[1,2] and Thomas Salez[2,3,4,*]

[1]*Department of Physics & Astronomy, McMaster University, Hamilton, Ontario L8S 4M1, Canada*
[2]*Laboratoire de Physico-Chimie Théorique, UMR CNRS Gulliver 7083, ESPCI Paris, PSL Research University, 75005 Paris, France*
[3]*Department of Mechanical and Aerospace Engineering, Princeton University, Princeton, New Jersey 08544, USA*
[4]*Global Station for Soft Matter, Global Institution for Collaborative Research and Education, Hokkaido University, Sapporo, Hokkaido 060-0808, Japan*

(Received 17 February 2016; published 11 October 2016)

We report on the capillary-driven leveling of a topographical perturbation at the surface of a freestanding liquid nanofilm. The width of a stepped surface profile is found to evolve as the square root of time. The hydrodynamic model is in excellent agreement with the experimental data. In addition to exhibiting an analogy with diffusive processes, this novel system serves as a precise nanoprobe for the rheology of liquids at interfaces in a configuration that avoids substrate effects.

DOI: 10.1103/PhysRevLett.117.167801

Continuum fluid dynamics provides a remarkably accurate description of flows from nanometric to astronomical length scales, and can accommodate a variety of forces and effects such as inertia, gravity, surface tension, viscosity, etc. Capillary-driven flows mediated by viscosity represent a particularly interesting situation as these two mechanisms dominate at small length scales and thus in several biological systems and technologically relevant applications [1,2]. They also underlie conceptually simple experiments that probe the physics at interfaces and in confinement, such as the motion of molecules in a liquid near a solid boundary [3], or the universal coalescence of droplets [4]. Moreover, the thin-film geometry allows for an important simplification since the in-plane flow dominates [5]. In this so-called lubrication approximation, the dynamics is solely controlled by the ratio of the film-air surface tension to the viscosity, known as the capillary velocity $v_c = \gamma/\eta$, and the film thickness, which sets the characteristic length scale.

Until now, research has been largely focused on thin films supported on solid substrates [6,7]. One way to probe the dynamics of such a film is to apply an external stress and to measure the departure from the initial state. Measurements can be achieved through a variety of experimental techniques such as the dynamic surface force apparatus [8], including substrate elasticity [9], nanoparticle embedding [10], electrohydrodynamic instability [11–13], unfavorable wetting conditions [3,14–19], and Marangoni flow [20,21]. Alternatively, the dynamics of a thin coating of liquid can be probed by starting with an out-of-equilibrium surface topography and observing the film as it relaxes towards equilibrium [22–28]. All the above approaches can be used to study physical properties such as the glass transition [10,23,25,28], viscoelasticity [27], and interfacial molecular friction [3,19].

In contrast to these studies, one could examine capillary-driven flows mediated by viscosity in a configuration with no substrate effect: a freestanding film. The flow in such a geometry has been previously studied for liquids with some internal structure that stabilizes the film against rupture, such as soap films [29–35], or liquid-crystal films [36–38], but this structure has necessarily a significant impact on the dynamics. Designing homogeneous isotropic freestanding liquid nanofilms presents experimental challenges in their creation, stability, and observation, as the techniques used for supported films typically do not work. Nevertheless, this geometry remains highly compelling as a way to study fundamental phenomena without substrate-induced effects. For instance, the glass-transition temperature reductions observed for supported films [39] are more pronounced for freestanding films [40]. Also, due to the absence of any liquid-substrate interaction, the confinement effects of polymeric liquids [41–44] may be addressed in an ideal way using freestanding films [45,46]. Furthermore, the interfaces of a freestanding film are the perfect realization of infinite-slip-length boundaries, and their behavior can shed light on theoretical predictions [47–50]. Finally, this technique has the potential to resolve questions such as the influence of thermal noise at interfaces [51–53].

In this Letter, we report on a novel capillary-leveling experiment involving freestanding stepped nanofilms. First, using atomic force microscopy (AFM), we empirically determine the scaling law for the width evolution of the prepared samples. Then, we derive a hydrodynamic model showing excellent agreement with experimental data. The only adjustable parameter is the capillary velocity, which allows the system to be used as a rheological nanoprobe. Finally, by performing simultaneous experiments on both supported and freestanding films, we self-consistently confirm the robustness of the technique.

Freestanding stepped films are prepared using a protocol inspired in part from Ref. [54]. Here, thin polystyrene (PS) films, with thicknesses in the 100–500 nm range, are spin coated from a dilute PS (Polymer Source, Canada, with a weight-averaged molecular weight of 55 kg/mol) solution in toluene onto freshly cleaved mica (Ted Pella, USA), and preannealed for at least 10 min on a hot stage (Linkham, UK) at 140 °C, well above the glass-transition temperature $T_g \approx 100$ °C of the material. After annealing, the films are floated onto a deionized water bath (18.2 MΩ cm, Pall, USA) and picked up onto custom-machined stainless steel grids. Each grid has 85 hexagonal holes (~1 mm across) that allow the simultaneous preparation of ~85 isolated freestanding samples. All results described here are obtained from the few films that remain stable against spontaneous rupture over the course of the entire experiment. After floating a film with thickness h_1 onto the grid, it is heated above T_g to remove wrinkles. A second film with thickness h_2 and a sharp edge [55] is then floated atop the first film, as schematically shown in Fig. 1(a). The freestanding stepped film is then annealed at 110 °C on the hot stage for a time t. To vertically equilibrate the pressure, the film rapidly symmetrizes into two mirrored steps as depicted in Fig. 1(b). Because the vertical length scale is orders of magnitude smaller than the typical horizontal one, the vertical symmetrization occurs rapidly on experimental time scales and is not resolved.

The presence of an excess interfacial area with respect to the flat equilibrium state drives flow, thus causing the profile to broaden laterally over time, as shown schematically in Fig. 1(c). After a chosen evolution time, each film is then cooled rapidly (> 90 °C/ min) from 110 °C to room temperature, deep into the glassy state, and the profile is imaged using AFM (Veeco Caliber, USA), with all sources of vibrations minimized. Then, the sample is placed back on the hot stage and rapidly heated above T_g to continue the leveling process. Because appreciable flow does not occur at room temperature, the film can be intermittently imaged this way.

Previous experiments on stepped films supported on a substrate [26] have shown that the width w of the profile increases with a 1/4 power law in time:

$$w \propto (v_c h_2^3 t)^{1/4}, \qquad \text{supported film}, \tag{1}$$

where h_2 is the thickness of the top film as in Fig. 1(a), and where the missing numerical prefactor depends on the aspect ratio h_2/h_1. Equation (1) is obtained from the capillary-driven thin-film equation [5–7], which results from the incompressible Stokes equation in the lubrication approximation, together with a no-slip boundary condition at the solid-liquid interface and no shear stress at the liquid-air interface. In that case, there is a nearly unidirectional flow with a parabolic velocity profile within the film.

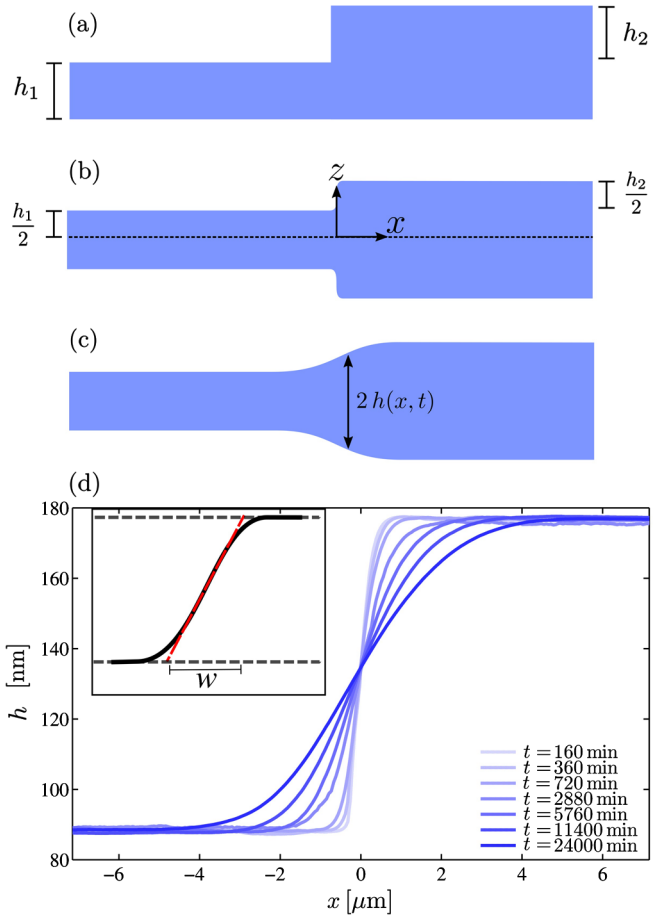

FIG. 1. (a) Schematic of a freestanding stepped film. (b) In the melt state, the profile quickly symmetrizes with respect to the central plane (dotted line) at $z = 0$. (c) The two mirrored steps broaden horizontally over time. The half-height profile $h(x, t)$ is recorded with AFM. (d) AFM profiles of a freestanding stepped film with $h_1 = h_2 = 176$ nm, for different times t spent above T_g. As sketched in the inset (arbitrary units), the profile width w is defined from the tangent (tilted dashed) line in the middle of the step and the film thickness.

For the freestanding stepped-film experiments studied here, a typical temporal evolution is shown in Fig. 1(d). To characterize the broadening, the width w of the profile [54] is defined [Fig. 1(d), inset] and recorded as a function of time. As seen in Fig. 2, the evolution is consistent with a $t^{1/2}$ power law. Also shown are the results for two other thicknesses (keeping $h_1 = h_2$). Each data set is then fit to $w = (Mt)^{1/2}$, where the mobility M is a free parameter that is found to scale linearly with h_2 (Fig. 2, inset). Using dimensional analysis, this empirically gives

$$w \propto (v_c h_2 t)^{1/2}, \qquad \text{freestanding film}, \tag{2}$$

where the missing prefactor is expected to depend on h_2/h_1. This scaling is similar to Eq. (1), but with a different power-law exponent. There is a stronger dependence on

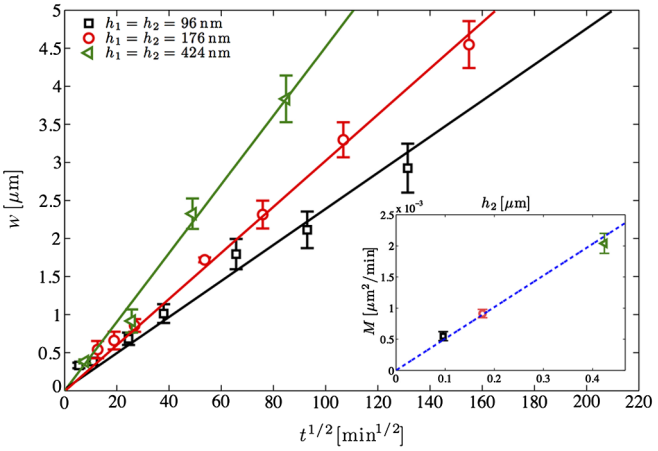

FIG. 2. Profile width w [Fig. 1(d), inset] as a function of the square root of time, $t^{1/2}$, for freestanding stepped films with $h_1 = h_2$. The open symbols are the measured widths for three different film thicknesses, as indicated. The solid lines are fits to $w = (Mt)^{1/2}$, where the mobility M is the fitting parameter. Inset: mobility as a function of thickness h_2, when $h_1 = h_2$. The dashed line is a linear fit.

time in freestanding films compared to supported films, which is consistent with the former flowing more easily due to the unconstrained boundaries.

Motivated by the empirical scaling of Eq. (2), we now turn to the theoretical description. Let us consider a symmetric freestanding film of total thickness $2h(x,t)$ [Fig. 1(c)] that viscously flows under the action of liquid-air surface tension. According to previous research on freestanding geometries [47,50] that invoke long-wave theory, the Young-Laplace equation in the small-slope approximation, as well as a no-shear boundary condition at each liquid-air interface, the mass and momentum conservations, respectively, lead to two coupled nonlinear equations:

$$h_t + (hu)_x = 0, \tag{3}$$

$$\frac{4}{v_c}(hu_x)_x + hh_{xxx} = 0, \tag{4}$$

where $u(x,t)$ is the horizontal component of the fluid velocity, and where the subscripts x and t indicate the corresponding partial derivatives. Note the equivalence of these equations to the ones describing the infinite-slip-length flow in supported films of thickness $h(x,t)$ [48,49], in the absence of disjoining pressure.

Let us linearize Eqs. (3) and (4) around the flat equilibrium state characterized by $h = h_{eq} = h_1/2 + h_2/4$ and $u = u_{eq} = 0$, where we assume that $h_2/4 \ll h_{eq}$. Doing so, and assuming that the stresses (and thus h_{xx} and u_x) vanish in the far field, one gets a diffusivelike freestanding thin-film equation for the film thickness:

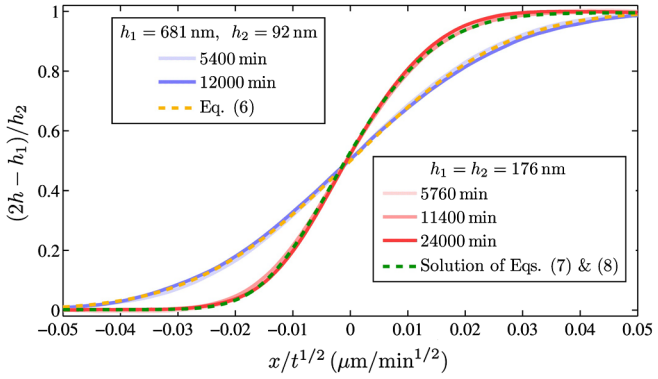

FIG. 3. Normalized long-time experimental height profiles as a function of the self-similar variable $x/t^{1/2}$, at several times and for two different geometries as indicated. The light (yellow) dashed line represents a fit using Eq. (6). The dark (green) dashed line indicates a fit using the numerical solution of Eqs. (7) and (8) for the $h_1 = h_2$ case.

$$h_t = \frac{v_c}{4}\left(\frac{h_1}{2} + \frac{h_2}{4}\right)h_{xx}. \tag{5}$$

Equation (5) can be solved analytically with the boundary conditions of Fig. 1(b), to arrive at

$$h(x,t) = \frac{h_1}{2} + \frac{h_2}{4}\left[1 + \mathrm{erf}\left(\frac{2x}{\sqrt{(2h_1 + h_2)v_c t}}\right)\right]. \tag{6}$$

As seen in Fig. 3, Eq. (6) fits the experimental data remarkably well for a sample with $h_1 = 681$ nm and $h_2 = 92$ nm, and the $x/t^{1/2}$ self-similarity is confirmed by the collapse of the profiles at two different times. The single fit parameter v_c will be studied in detail below.

We now turn to the general nonlinear case. Let us first nondimensionalize Eqs. (3) and (4) through $h = Hh_1/2$, $x = Xh_1/2$, $u = Uv_c/4$, and $t = 2Th_1/v_c$. Inspired by the linear case above, and by the empirical scaling of Eq. (2), we make the following self-similarity ansatz [56]: $H(X,T) = F(S)$, and $U(X,T) = Q(S)/T^{1/2}$, where $S = X/T^{1/2}$. Assuming further that Q', F', and F'' vanish as $S \to -\infty$, while by construction $\lim_{S\to-\infty} F = 1$, Eqs. (3) and (4) become

$$Q' = \frac{SF'}{2F} - \frac{QF'}{F}, \tag{7}$$

$$F'' = \frac{F'^2}{2F} - Q'. \tag{8}$$

We solve these equations using a one-parameter shooting method. In fact, as $S \to -\infty$, Eqs. (7) and (8) can be linearized around the boundary conditions $F = 1$ and $Q = 0$. The approximate far-field solution is $F \simeq 1 + c[1 + \mathrm{erf}(S/2)]$, together with $Q = -F'$, where c is an unknown constant. This analysis allows us to

evaluate F and Q at the left boundary of the integration domain ($-S \gg 1$). For an arbitrary c, one can thus integrate Eqs. (7) and (8) numerically using a Runge-Kutta scheme. We then shoot over c until the numerical solution reaches the proper limit, $\lim_{S\to+\infty} F = 1 + h_2/h_1$, at the right boundary of the integration domain ($S \gg 1$). Figure 3 shows the long-time experimental profiles of the $h_1 = h_2 =$ 176 nm geometry of Fig. 1(d). The normalized height is plotted against the self-similar variable $x/t^{1/2}$, for three different annealing times. The profiles collapse onto a single master curve—thus confirming the self-similarity ansatz—and are in full agreement with the numerical solution. The vertical discrepancy is less than 1 nm, even after the hundreds of hours of flow in the experiments, and there is a comparable level of agreement (not shown) for the two other $h_1 = h_2$ geometries introduced in Fig. 2.

A final self-consistency check is performed in order to ensure the accuracy on the single fit parameter v_c extracted from the comparison with theory. As a material property of the film in contact with air, it should not depend on the presence of an additional substrate-film interface. Stepped PS films (55 kg/mol, $h_1 = h_2 = 390$ nm) are thus prepared in freestanding and substrate-supported (on silicon wafers or ~4 μm-thick polysulfone films) configurations. Both are annealed side by side, at the same time, in a vacuum oven at 120 °C. The profiles are measured after 735 and 1485 min to confirm self-similarity. Figure 4(a) shows the results for the supported case. The normalized height profile is plotted as a function of the self-similar variable $x/t^{1/4}$ of Eq. (1). The numerical profile [57] is fit to the experimental data with one single free parameter: $v_c = 0.068 \pm 0.010$ μm/ min. Figure 4(b) shows the results for the freestanding case. The normalized height profile is plotted as a function of the self-similar variable $x/t^{1/2}$ of Eq. (2). The numerical solution of Eqs. (7) and (8) described above is fit to the experimental data with one single free parameter: $v_c = 0.087 \pm 0.012$ μm/ min. Note the difference between the profile shapes of both cases, reflecting the different orders in the governing equations. Together with the excellent fit qualities, the fact that both cases give the same capillary velocity within experimental error proves (i) the robustness of the freestanding stepped-film technique as a rheological nanoprobe, and (ii) the validity of the hydrodynamic model.

In conclusion, we report on capillary-driven viscous flow in polystyrene freestanding stepped nanofilms. Above the glass-transition temperature, the surface profiles broaden with a characteristic $t^{1/2}$ power law, as measured by AFM. This response differs significantly from the $t^{1/4}$ power law of substrate-supported films with a no-slip liquid-solid boundary condition. The hydrodynamic model is found to be in excellent agreement with experimental data. Finally, the capillary velocity γ/η is robustly and accurately extracted from the comparison with theory. We expect this novel system to be of fundamental interest for three reasons: first, it presents a striking analogy with diffusive processes; second, it embodies a perfect realization of the infinite-slip-length limit of low-Reynolds-number thin-film hydrodynamics and, as such, it is a test of the associated theoretical predictions; third, by avoiding substrate-induced effects, it may serve as a precise nanoprobe for addressing fundamental questions about complex fluids and glass formers in confinement and at interfaces.

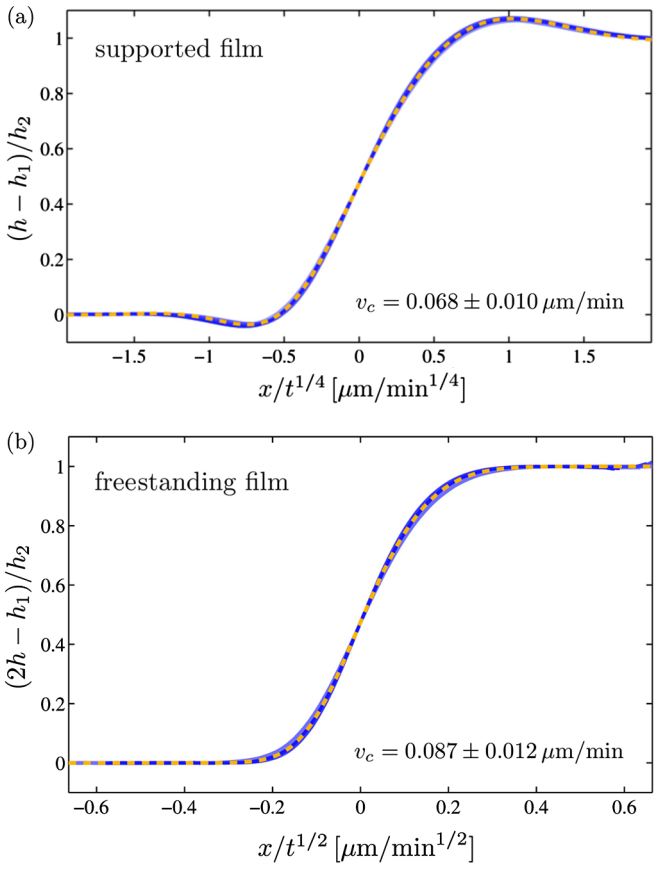

FIG. 4. (a) Normalized long-time experimental height profiles (solid lines) of supported PS stepped films (55 kg/mol, $h_1 = h_2 = 390$ nm) as a function of the self-similar variable $x/t^{1/4}$ of Eq. (1), for ten samples and two different times. The numerical solution [57] is fit (dashed line) to the experimental profiles with v_c as the free parameter. (b) Normalized long-time experimental height profiles (solid lines) of freestanding PS stepped films (55 kg/mol, $h_1 = h_2 = 390$ nm) as a function of the self-similar variable $x/t^{1/2}$ of Eq. (2), for 12 samples and two different times. The numerical solution of Eqs. (7) and (8), for the $h_1 = h_2$ case, is fit (dashed line) to the experimental profiles with v_c as the free parameter.

The authors thank Martin Brinkmann and René Ledesma-Alonso for interesting discussions, and gratefully acknowledge financial support from NSERC of Canada and the Global Station for Soft Matter, a project of the Global Institution for Collaborative Research and Education at Hokkaido University.

*thomas.salez@espci.fr

[1] P. Tabeling, *Introduction to Microfluidics* (Oxford University Press, New York, 2005).
[2] K. Jacobs, R. Seemann, and S. Herminghaus, in *Polymer Thin Films*, edited by O. K. C. Tsui and T. P. Russell (World Scientific, Singapore, 2008), Chap. 10, pp. 243–265.
[3] O. Bäumchen and K. Jacobs, J. Phys. Condens. Matter **22**, 033102 (2010).
[4] J. F. Hernández-Sánchez, L. A. Lubbers, A. Eddi, and J. H. Snoeijer, Phys. Rev. Lett. **109**, 184502 (2012).
[5] R. Blossey, *Thin Liquid Films: Dewetting and Polymer Flow* (Springer, New York, 2012).
[6] A. Oron, S. Davis, and S. Bankoff, Rev. Mod. Phys. **69**, 931 (1997).
[7] R. Craster and O. Matar, Rev. Mod. Phys. **81**, 1131 (2009).
[8] J. N. Israelachvili, P. M. McGuiggan, and A. M. Homola, Science **240**, 189 (1988).
[9] R. Villey, E. Martinot, C. Cottin-Bizonne, M. Phaner-Goutorbe, L. Léger, F. Restagno, and E. Charlaix, Phys. Rev. Lett. **111**, 215701 (2013).
[10] J. H. Teichroeb and J. A. Forrest, Phys. Rev. Lett. **91**, 016104 (2003).
[11] E. Schaffer, T. Thurn-Albrecht, T. Russell, and U. Steiner, Nature (London) **403**, 874 (2000).
[12] M. D. Morariu, N. E. Voicu, E. Schäffer, Z. Lin, T. P. Russell, and U. Steiner, Nat. Mater. **2**, 48 (2003).
[13] N. Voicu, S. Harkema, and U. Steiner, Adv. Funct. Mater. **16**, 926 (2006).
[14] D. J. Srolovitz and S. A. Safran, J. Appl. Phys. **60**, 255 (1986).
[15] F. Wyart and J. Daillant, Can. J. Phys. **68**, 1084 (1990).
[16] R. Seemann, S. Herminghaus, and K. Jacobs, Phys. Rev. Lett. **87**, 196101 (2001).
[17] G. Reiter, M. Hamieh, P. Damman, S. Sclavons, S. Gabriele, T. Vilmin, and E. Raphaël, Nat. Mater. **4**, 754 (2005).
[18] X.-C. Chen, H.-M. Li, F. Fang, Y.-W. Wu, M. Wang, G.-B. Ma, Y.-Q. Ma, D.-J. Shu, and R.-W. Peng, Adv. Mater. **24**, 2637 (2012).
[19] O. Bäumchen, R. Fetzer, and K. Jacobs, Phys. Rev. Lett. **103**, 247801 (2009).
[20] J. M. Katzenstein, D. W. Janes, J. D. Cushen, N. B. Hira, D. L. McGuffin, N. A. Prisco, and C. J. Ellison, ACS Macro Lett. **1**, 1150 (2012).
[21] C. B. Kim, D. W. Janes, D. L. McGuffin, and C. J. Ellison, J. Polym. Sci., Part B: Polym. Phys. **52**, 1195 (2014).
[22] O. K. C. Tsui, Y. J. Wang, F. K. Lee, C.-H. Lam, and Z. Yang, Macromolecules **41**, 1465 (2008).
[23] Z. Fakhraai and J. A. Forrest, Science **319**, 600 (2008).
[24] T. Leveder, S. Landis, and L. Davoust, Appl. Phys. Lett. **92**, 013107 (2008).
[25] Z. Yang, Y. Fujii, F. K. Lee, C.-H. Lam, and O. K. C. Tsui, Science **328**, 1676 (2010).
[26] J. D. McGraw, T. Salez, O. Bäumchen, E. Raphaël, and K. Dalnoki-Veress, Phys. Rev. Lett. **109**, 128303 (2012).
[27] E. Rognin, S. Landis, and L. Davoust, J. Vac. Sci. Technol., B **30**, 011602 (2012).
[28] Y. Chai, T. Salez, J. D. McGraw, M. Benzaquen, K. Dalnoki-Veress, E. Raphaël, and J. A. Forrest, Science **343**, 994 (2014).
[29] M. A. Rutgers, X.-l. Wu, R. Bhagavatula, A. A. Petersen, and W. I. Goldburg, Phys. Fluids **8**, 2847 (1996).
[30] V. K. Horváth, J. R. Cressman, W. I. Goldburg, and X. L. Wu, Phys. Rev. E **61**, R4702 (2000).
[31] A. Aradian, E. Raphaël, and P.-G. de Gennes, Europhys. Lett. **55**, 834 (2001).
[32] D. Georgiev and P. Vorobieff, Rev. Sci. Instrum. **73**, 1177 (2002).
[33] H. Diamant, J. Phys. Soc. Jpn. **78**, 041002 (2009).
[34] J. Seiwert, M. Monloubou, B. Dollet, and I. Cantat, Phys. Rev. Lett. **111**, 094501 (2013).
[35] M. J. Huang, C. Y. Wen, I. C. Lee, and C. H. Tsai, Phys. Fluids **16**, 3975 (2004).
[36] K. Harth, A. Eremin, and R. Stannarius, Soft Matter **7**, 2858 (2011).
[37] A. Eremin, C. Bohley, and R. Stannarius, Phys. Rev. E **74**, 040701(R) (2006).
[38] R. Stannarius, C. Bohley, and A. Eremin, Phys. Rev. Lett. **97**, 097802 (2006).
[39] J. L. Keddie, R. A. L. Jones, and R. A. Cory, Europhys. Lett. **27**, 59 (1994).
[40] J. A. Forrest, K. Dalnoki-Veress, J. R. Stevens, and J. R. Dutcher, Phys. Rev. Lett. **77**, 2002 (1996).
[41] A. Silberberg, J. Colloid Interface Sci. **90**, 86 (1982).
[42] F. Brochard Wyart and P.-G. de Gennes, Eur. Phys. J. E **1**, 93 (2000).
[43] H. Bodiguel and C. Fretigny, Phys. Rev. Lett. **97**, 266105 (2006).
[44] K. Shin, S. Obukhov, J.-T. Chen, J. Huh, Y. Hwang, S. Mok, P. Dobriyal, P. Thiyagarajan, and T. Russell, Nat. Mater. **6**, 961 (2007).
[45] K. Dalnoki-Veress, J. A. Forrest, P. G. de Gennes, and J. R. Dutcher, J. Phys. IV (France) **10**, Pr7 (2000).
[46] L. Si, M. V. Massa, K. Dalnoki-Veress, H. R. Brown, and R. A. L. Jones, Phys. Rev. Lett. **94**, 127801 (2005).
[47] J. Eggers, Rev. Mod. Phys. **69**, 865 (1997).
[48] K. Kargupta, A. Sharma, and R. Khanna, Langmuir **20**, 244 (2004).
[49] A. Münch, B. Wagner, and T. P. Witelski, J. Eng. Math. **53**, 359 (2005).
[50] P. D. Howell and H. A. Stone, Eur. J. Appl. Math. **16**, 569 (2005).
[51] B. Davidovitch, E. Moro, and H. A. Stone, Phys. Rev. Lett. **95**, 244505 (2005).
[52] G. Grün, K. Mecke, and M. Rauscher, J. Stat. Phys. **122**, 1261 (2006).
[53] Y. Hennequin, D. G. A. L. Aarts, J. H. van der Wiel, G. Wegdam, J. Eggers, H. N. W. Lekkerkerker, and D. Bonn, Phys. Rev. Lett. **97**, 244502 (2006).
[54] J. D. McGraw, N. M. Jago, and K. Dalnoki-Veress, Soft Matter **7**, 7832 (2011).
[55] O. Bäumchen, M. Benzaquen, T. Salez, J. D. McGraw, M. Backholm, P. Fowler, E. Raphaël, and K. Dalnoki-Veress, Phys. Rev. E **88**, 035001 (2013).
[56] G. I. Barenblatt, *Scaling, Self-similarity, and Intermediate Asymptotics* (Cambridge University Press, Cambridge, England, 1996).
[57] T. Salez, J. D. McGraw, S. L. Cormier, O. Bäumchen, K. Dalnoki-Veress, and E. Raphaël, Eur. Phys. J. E **35**, 114 (2012).